Int. J. Heat Mass Transfer. Vol. 31, No. 6, pp. 1127–1135, 1988
Printed in Great Britain

0017–9310/88 $3.00 + 0.00

A mathematical model of the pool boiling nucleation site density in terms of the surface characteristics

S. R. YANG
Northeast Institute of Electric Power Engineering, Jilin City, People's Republic of China

and

R. H. KIM
Mechanical Engineering and Engineering Science, University of North Carolina at Charlotte, Charlotte, NC 28223, U.S.A.

(*Received* 14 *October* 1986 *and in final form* 31 *August* 1987)

Abstract—Dependence of active nucleation site density on boiling surface conditions are developed in a form of $N = N \cdot \phi(\beta) \cdot \phi(r)$. The average cavity density N is obtained from the measurement of the boiling surface. The distribution functions $\phi(\beta)$ and $\phi(r)$ are of the form

$$\phi(\beta) = \int_0^{\theta/2} f(\beta)\,\mathrm{d}\beta, \quad \phi(r) = \int_{r_{\min}}^{r_{\max}} f(r)\,\mathrm{d}r.$$

The probability density function of the cavity mouth radius $f(r)$ and the cone angle $f(\beta)$ are obtained through a statistical treatment based on the measured cavities by a scanning electron microscope and a differential interference contrast microscope. The limits of integrations are given by the entrapment mechanism. The agreement between the result of the analysis and experimental data is good.

INTRODUCTION

THE EFFECTS of boiling surface conditions on pool boiling heat transfer have been studied for at least 30 years. Corty and Foust [1] and Griffith and Wallis [2] indicated that the microroughness of the boiling surface had a profound effect on the position and slope of the nucleate boiling in the mid 1950s and the beginning of the 1960s. Clark *et al.* [3] confirmed this and it was later verified by Cornwell [4] and Sultan and Judd [5] that cavities and scratches were in fact nucleation sites. In the early 1970s Porchey *et al.* [6] and Nail *et al.* [7] using a scanning electron microscope (SEM) examined the boiling surface. Kopp [8] and Vaynshteyn *et al.* [9] tried to depict the characteristics of boiling surface microroughness by statistical parameters and correlated with boiling heat transfer. Gaertner [10] statistically examined the data of ref. [11] and pointed out that the active nucleation site spatial distribution fits the Poisson distribution. Rohsenow [12], using the data provided by Griffith and Wallis [2], estimated that the nucleation site density could be obtained from the integration of a cavity distribution function in terms of cavity radius. Gorenflo *et al.* [13] and Schlünder [14] proposed that the size distribution is a combined power series with the exponential function, and then Bier *et al.* [15] introduced the distribution function into the correlation. In the late 1950s, Bankoff [16] proposed the trapping mechanism of how a conical cavity entraps the gas–vapor in it. This model was later developed by Lorenz [17]. Shoukri and Judd [18] confirmed the minimum radius of equation (2) experimentally. Hsu [19], using the assumption of thermal layer thickness, determined the maximum and minimum size of nucleation sites. Mizukami [20] proposed a stability criterion for vapor bubble nuclei, and pointed out that the liquid–vapor interface can be stable only at the cavity mouth. Now, it has been generally agreed [2, 21, 22] that the pool boiling active nucleation site density can be determined as a function of the cavity radius in the form

$$N = C(r_{\min})^m \tag{1}$$

where N is the active nucleation site density, $r_{\min}$ the minimum cavity radius at a specified condition, and C and m are constants characterizing the boiling surface. The minimum cavity radius $r_{\min}$ is defined as

$$r_{\min} = 2\sigma T_{\mathrm{sat}} v_{\mathrm{fg}}/(h_{\mathrm{fg}} \cdot \Delta T). \tag{2}$$

Mikic and Rohsenow [23] and Lorenz *et al.* [24] correlated the nucleation site density with the radius of the cavity in a different form

$$N = C_1(r_L/r_{\min})^m \tag{3}$$

where r_L is a radius for which N is one per unit area, and C_1 is a dimensional constant (1/unit area).

Bier *et al.* [15] proposed another form of the relationship

NOMENCLATURE

C	constant
C_1	constant
E	maximum error
ER	allowable error used in equation (14)
F_g	difference of gravity force between liquid and vapor [N]
F_s	surface tension force [N]
g	acceleration of gravity [m s^{-2}]
h	height defined in Fig. 7 [m]
h_{fg}	latent heat [W kg^{-1} °C^{-1}]
K	constant used in equation (16)
m	constant
N	active nucleation site density [site mm^{-2}]
r	radius
s	standard deviation
ΔT	boiling surface superheat [°C]
v	specific volume.

Greek symbols

β	half of cone angle
δ	secondary emission coefficient
θ	contact angle
λ	statistical parameter defined in equation (5)
$\Delta\rho$	density difference between liquid and saturated vapor
σ	surface tension [N m^{-1}]
ϕ	function defined by $\int f(x_i)\,dx_i$, $x_i = r, \beta$
χ	parameter for chi-square test.

Subscripts

c	at the mouth of the cavity
c	interface radius defined in Fig. 7
fg	liquid–vapor phase
L	radius defined in equation (3)
max	maximum value
min	minimum value
s	structure upper limit
sat	saturation state
st	maximum value of r defined in equation (4).

$$\ln N = \ln N_{max}(1-(r/r_{st})^m) \quad (4)$$

where N_{max} is the maximum value of N ($r = 0$) and r_{st} is the maximum value of r, which corresponds to the beginning of nucleation ($N = 1$).

Even though all the previous works have significant theories and improvements, none of them seems to reflect accurately the dependence of the nucleation site density on the boiling surface conditions. Also, it has been pointed out that equation (1) is difficult to use in practice [25] and furthermore, equations (1), (3), and (4) do not reveal the mechanism responsible.

The present work determines a mathematical expression of the active nucleation site density in terms of the cavity mouth radius and cone angle and studies the effect of the surface micro characteristics on the nucleation site density.

This work is based on the following points.

(1) The cavity, consisting of a crevice and or a scratch, containing gas and/or vapor is the possible active nucleation site. This was noted by Corty and Foust [1] and confirmed by Clark *et al.* [3], Gaertner and Westwater [11] and Cornwell [4].

(2) The minimum cavity radius which can be activated at a given surface superheat T is expressed as

$$r_{min} = 2\sigma T_{sat} v_{fg}/(h_{fg} \cdot \Delta T) \quad (2)$$

which was postulated by Griffith and Wallis [2].

In this paper, a description of the procedure for obtaining the cavity probability density function is offered in terms of the radius and cone angle. Then based on the trapping mechanism [16, 17] the range of active nucleation sites is determined. Finally the active nucleation site density is postulated to depend on the cavity distribution function and compares the results of this hypothesis with the experimental data and previous works.

THE SAMPLE DESIGN

The heating element is made of stainless steel. The surface of the heating element is 33 mm in diameter and 7 mm in height. After following the surface preparation procedure, which will be described later, the cavities on the surface of the heating element were observed by an SEM and a differential interference contrast microscope (DIC) to get the cavity probability density function in terms of the cavity radius and cone angle. Measurements of cavity characteristics of the boiling surface have been made by the SEM before. Shoukri and Judd [18] used a Watson 16 mm interference objective and a microscope objective lens with a built-in interferometer for the examination of surfaces. This is the same kind of device as the DIC. However, the DIC used by the authors seems to be an advanced and dedicated device for surface conditions. The DIC is an optical interference microscope for examining the morphology of semiconductor wafer surfaces. Because of the excellent in-depth resolution of the DIC, focusing can be made to the surface under consideration and the micrometer is recorded for the vertical adjustment. Then a new vertical adjustment is made for the deeper point of the cavity to be in focus and the micrometer position is recorded. Using the difference of the vertical micrometer readings, one may obtain the cavity depth based on the calibrated

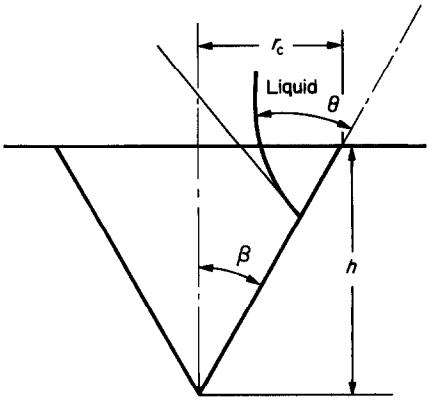

FIG. 1. The entrapment of the cavity.

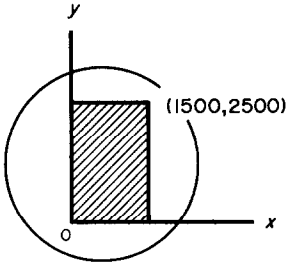

FIG. 2. Coordinates of areas for the SEM.

scale. The cavity mouth radius is measured by the graduation of the eyepiece. Both the depth scale and the mouth radius scale are calibrated before measurement. From the depth h and the mouth radius r_c for a cavity the cone angle β shown in Fig. 1 is obtained, i.e. $\beta = \tan^{-1}(r_c/h)$. Then apparatus similar to that of Clark *et al.* [3] is used to check the validity of the assumptions and analysis employed for the present work.

Due to the limit of the SEM operation range, only the central area of 15×25 mm is examined. The surface was prepared before examination as follows. First, it was ground with wet sandpaper from 240 grit to 600 grit. Then it was polished with 1 μm (ferric oxide) and 3 μm (aluminum oxide) by a cotton polishing wheel. After those procedures, the surface had the appearance of a mirror.

It is apparent that the statistical approach is a better technique to deal with the cavities on the surface. Random locations on the surface area were determined with a microcomputer based on the identification of the small area by its center coordinates as shown in Fig. 2. For example, since the SEM and DIC determine the radius and the cone angle of the cavity in the designated area, the area is identified by an eight-digit number, the first four digits representing its abscissa, the second four digits representing its ordinate. According to the identification of the area, two axis controls of the SEM and DIC on the plane of the surface were adjusted to place the eyepiece on the randomized area.

Then measurement of the cavity was made in the area. Most of the black spots on the SEM screen were not real cavities when examined by the DIC. A typical result of the cavity is shown in Figs. 3 and 4. The DIC screen shows the three-dimensional features somewhat, since carbon has a smaller secondary emission coefficient δ than iron and chromium [26], so the carbon crystalloid looks darker than iron and chromium does on the SEM screen. Roughly one-third of the black spots are cavities. Tables 1 and 2 summarize the observed data of the radius and cone angle values. The population size, the level of significance, and the finite population correction factor for the randomization are 2×10^4–3×10^4, 0.01 μm and 1.0, respectively [27].

The cavity distribution is plotted in terms of the radius of the cavity in Fig. 5 and in terms of the cavity angle in Fig. 6. It is assumed that the cavity distribution and the angle distribution fit the Poisson and normal distributions, respectively. By applying the Chi-square test on the measurements, the probability density function of the cavity radius for the specimen surface takes the form

$$f(r) = \lambda e^{-\lambda r}, \quad \lambda = 0.9797 \tag{5}$$

and the probability density function of the cavity cone angle has the form

$$f(\beta) = ((2\pi)^{1/2}s)^{-1} \exp(-(\beta-\bar{\beta})^2/(2s)),$$
$$s = 0.2849, \quad \bar{\beta} = 0.3744. \tag{6}$$

The probability density functions and the measured values of the radius and cone angle are shown in Figs. 5 and 6. Details of the statistical analysis are provided in ref. [27].

MECHANISM OF ENTRAPMENT OF GAS–VAPOR IN A CAVITY

According to the gas–vapor trapping mechanism proposed by Bankoff [16] and later developed by Lorenz [17], the decisive conditions of gas–vapor entrapment for a cavity are the mouth radius and the cone angle of the cavity. These two conditions are summarized below.

(1) Based on the investigations of Bankoff and Lorenz [16, 17] (Fig. 1), and the effective cavity cone angle of the entrapment for a conical cavity of radius r_c and cone angle 2β, the entrapment condition can be written as

$$\theta > 2\beta \tag{7}$$

where θ is the contact angle of the liquid and the surface.

This means that the cavities with $\beta \geqslant \theta/2$ cannot entrap gas or vapor in it, and as a result, these cavities cannot become active nucleation sites. Only those cavities for which $\beta < \theta/2$ have the possibility of becoming active nucleation sites provided that the cavities are assumed to be conical in shape. Therefore,

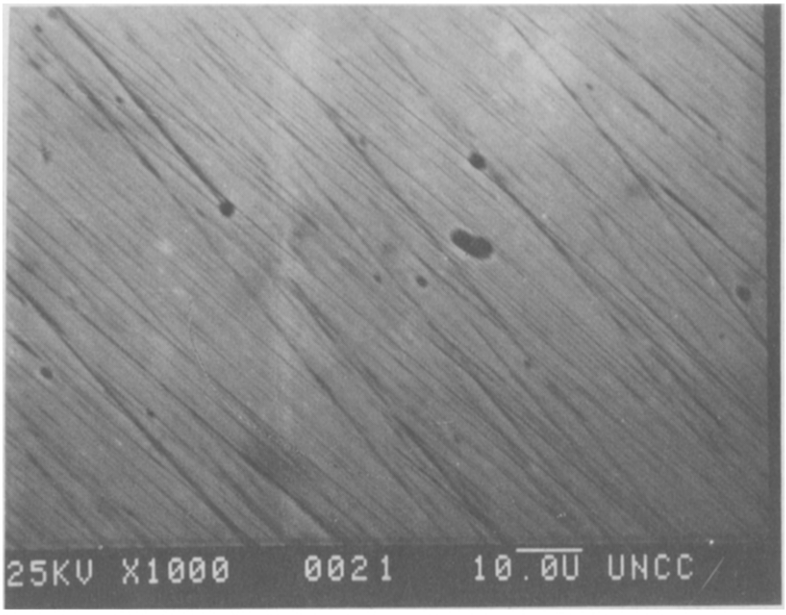

FIG. 3. Example of cavity features from the SEM.

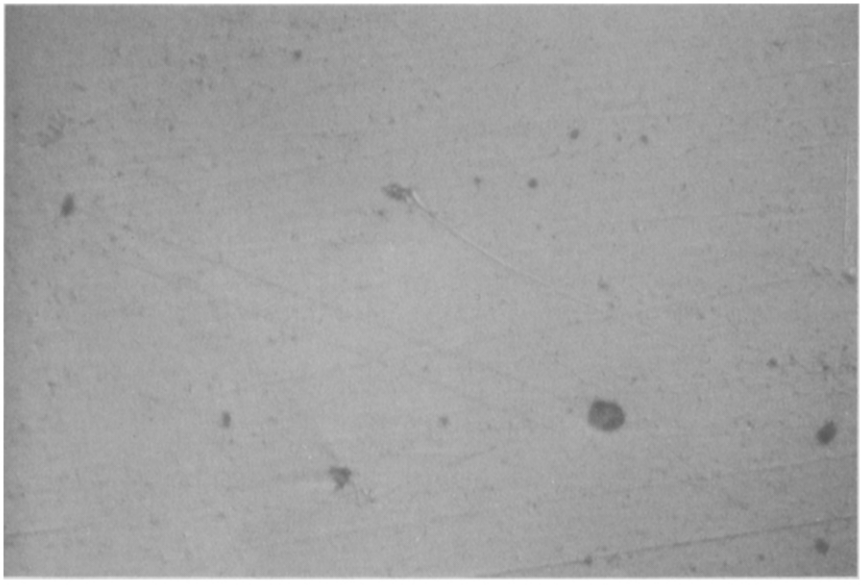

FIG. 4. Example of cavity features from the DIC.

among the whole cavities of the boiling surface only the following part of it can meet the condition

$$N = \bar{N}\phi(\beta) = \bar{N}\int_0^{\theta/2} f(\beta)\,\mathrm{d}\beta \tag{8}$$

where $f(\beta)$ is the probability density function of the cavity in terms of the cavity cone angle, expressed by equation (6) and $\bar{N}$ is the average cavity density based on the measured data. For example, for the stainless steel–water combination with contact angle $\theta = 65°$ (under a temperature of 20°C and air) [28] if the probability density function is computed with equation (6), then

$$\phi(\beta) = \int_0^{\theta/2} f(\beta)\,\mathrm{d}\beta = 0.2508.$$

That means only about a quarter of the cavities have the possibility of becoming nucleation sites.

(2) In the range of active nucleation site radius, Mizukami [20] indicated that the liquid–vapor interface can be stable only at the mouth of the cavity.

Table 1. Number of cavity in cavity radius ranges

No.	Range of cavity mouth radius (μm)	Middle point value of radius (μm)	Number of cavity within the range
1	0.3448–0.5173	0.4311	12
2	0.5173–0.6897	0.6035	4
3	0.6897–0.8621	0.7759	8
4	0.8621–1.0345	0.9483	7
5	1.0345–1.2069	1.1207	3
6	1.2069–1.3793	1.2931	3
7	1.3793–1.5518	1.4655	5
8	1.5518–1.7242	1.6380	4
9	1.7242–1.8966	1.8104	0
10	1.8966–2.0690	1.9828	0
11	2.0690–2.2414	2.1552	2
12	2.2414–2.4138	2.3276	1
13	2.4138–2.5862	2.5000	0
14	2.5862–2.7587	2.6724	0
15	2.7587–2.9313	2.8449	1
16	2.9313–3.1035	3.0175	0

$\chi^2 = 5.9286 < \chi^2_{0.01}(2) = 9.21.$

Table 2. Number of cavity in cone angle ranges

No.	Range of cavity cone angle (rad)	Middle point value (rad)	Number within the range
1	0–0.1205	0.06	8
2	0.1205–0.2405	0.18	11
3	0.2405–0.3605	0.30	12
4	0.3605–0.4805	0.42	3
5	0.4805–0.6005	0.54	10
6	0.6005–0.7205	0.66	0
7	0.7205–0.8405	0.78	1
8	0.8405–0.9605	0.90	2
9	0.9605–1.0805	1.02	1
10	1.0805–1.2005	1.14	1
11	1.2005–1.3205	1.26	1
12	1.3205–1.4405	1.38	0

$\chi^2 = 1.1078 < \chi^2_{0.01}(1) = 6.635.$

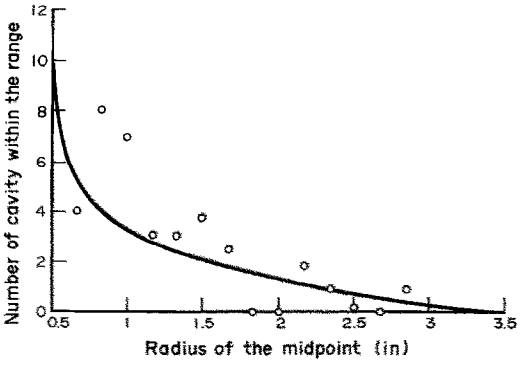

FIG. 5. Probability density function of cavity radius.

From the geometric relationship of Fig. 7, the stable interface radius r_e and the cavity mouth radius r_c have the relationship

$$r_e = -r_c/\cos(\theta-\beta) \tag{9}$$

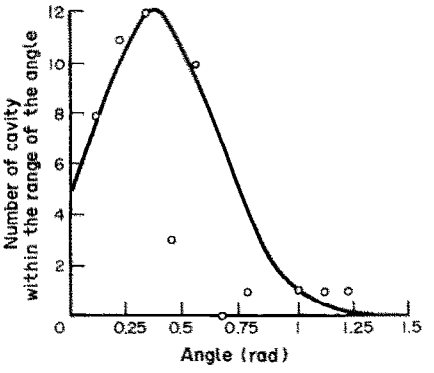

FIG. 6. Probability density function of cavity cone angle.

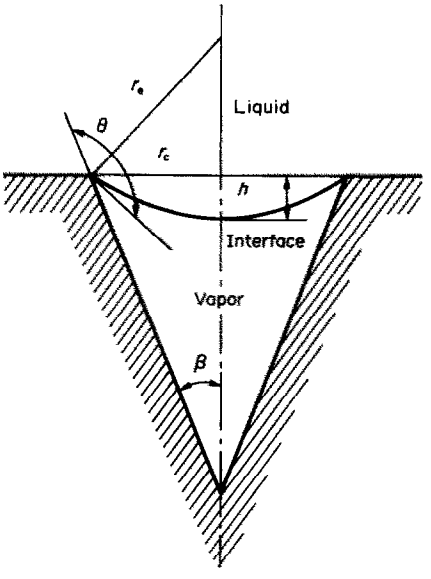

FIG. 7. Geometric relationship of interface in cavity.

where the negative value of r_e means that the liquid–vapor interface has a concave meniscus.

When liquid advances over a conical cavity, for the cavity cone angle β, the gas–vapor interface will sit at the cavity mouth, as shown in Fig. 7. In the steady state, the resultant of forces acting on the interface should be equal to zero

$$2\pi r_c\sigma\cos(\theta-\beta)+(\Delta\rho)g(\pi/6)h(3r_c^2+h^2)=0 \tag{10}$$

where $\Delta\rho$ is the density difference between liquid and vapor in kg m^{-3} and σ is the surface tension in N m^{-1}. Here the force downward is positive and h can be obtained from the geometric relationship as follows:

$$h = (\sin(\theta-\beta)-1)r_c/\cos(\theta-\beta). \tag{11}$$

Substituting equation (11) into equation (10) yields

$$r_c = \sqrt{\left\{4\sigma\cos^2(\theta-\beta)\Big/\left[(\Delta\rho)g(1-\sin(\theta-\beta))\times\left(1+\frac{(\sin(\theta-\beta)-1)^2}{3\cos^2(\theta-\beta)}\right)\right]\right\}}. \tag{12}$$

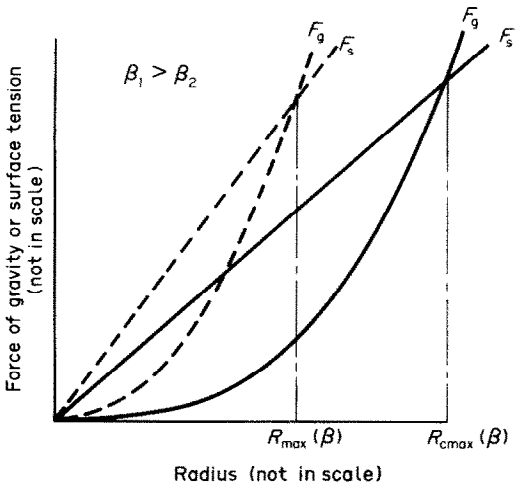

FIG. 8. Gravity force and surface tension force vs cavity radius.

This is the maximum entrapment radius for a cavity with a cone angle β under a certain liquid–surface combination of contact angle θ and surface tension σ. Let us designate this as r_{max}. This r_{max} implies that cavities of radius greater than r_{max} obtained by equation (12) cannot entrap gas–vapor in it. This is further explained as follows.

Figure 8 shows variations of the gravity difference

$$F_g = (\Delta\rho)\, g(\pi/6)h(3r_c^2 + h^2)$$

and the surface tension

$$F_s = 2\pi r_c \sigma \cos(\theta - \beta)$$

of equation (10) vs the cavity mouth radius. The gravity difference F_g is dependent on the cube of the cavity mouth radius, but the surface tension only depends on the cavity mouth radius linearly. As the radius increases, the increment of F_g is greater than that of F_s. When a cavity has a radius $r_c > r_{max}$, F_g will be larger than F_s and the cavity will be flooded.

For a given liquid–surface, the value of r_{max} depends on the cavity cone angle β. The larger the value of β, the smaller the value of r_{max}. The cavities of radii less than r_{max} can have a stable interface at the cavity mouth. If the mouth radius is less than

$$r_{min} = 2\sigma T_{sat} v_{fg}/(h_{fg} \cdot \Delta T) \qquad (2)$$

the cavity still cannot become an active nucleation site regardless of the fact that the cavity entrapped the gas–vapor in it. This is because the surface superheat ΔT is not enough to initiate the growth of a bubble. So, for an active nucleation site, the radius of equation (2) seems to be the lower limit of the active nucleation site.

Up to now, it has been demonstrated that among the cavities only those with a mouth radii between r_{min} and r_{max} can become active nucleation sites. That is, the active nucleation site is expressed as

$$\phi(r) = \int_{r_{min}}^{r_{max}} f(r)\, dr = \int_{r_{min}}^{r_{max}} \lambda e^{-\lambda r}\, dr. \qquad (13)$$

The maximum entrapment radius determined by equation (12) comes from the entrapment mechanism. The value obtained is much greater than the technical grade metal cavity radius. For example, for the stainless steel–water combination, if a cavity cone angle β is 20°, then $r_{max} = 2.03 \times 10^3$ μm, but the magnitude of the technical grade metal cavity radii is about 10^2 μm. A similar situation to this has been pointed out by Kopp [30]. For a particular boiling surface, depending on its material and finish, there is another upper limit of cavity radius. Let us call this limit the structure upper limit or the upper limit r_s. This is determined as follows. For practical purposes, let us say that when $e^{-\lambda r_s}/e^{-\lambda r_{min}}$ is less than an allowable error, let us say 0.10%, the value of $e^{-\lambda r_s}$ can be neglected, that is

$$\phi(r) = e^{-\lambda r_{min}} - e^{-\lambda r_s} \cong e^{-\lambda r_{min}}.$$

From this condition, when λ and r_{min} are given, the upper limit r_s may be determined as

$$r_s < (\ln ER)/\lambda - r_{min} \qquad (14)$$

where ER is the allowable error. For example if $ER = 0.1\%$ with other previously given variables $r_s = 4.54$ μm. Using r_s as the upper limit for integrating equation (13) instead of r_{max} the active nucleation site density is not affected anymore. So, equation (13) can be written as

$$\phi(r) = \int_{r_{min}}^{r_s} \lambda e^{-\lambda r}\, dr. \qquad (13a)$$

This can be easily understood, simply because after determining the parameter, through statistical analysis and r_s from equation (14), the probability of a cavity having a radius greater than r_s is almost equal to zero.

THE RELATIONSHIP BETWEEN THE NUCLEATION SITE DENSITY AND THE SURFACE CHARACTERISTICS

From the previous sections, it has been demonstrated that among the cavities on the boiling surface, only a part of them can entrap gas–vapor. For these cavities which have entrapped gas–vapor, if their mouth radius is in the range from r_{min} to r_s, they will become active nucleation sites. The real active nucleation site density then can be expressed as

$$N = \bar{N} \int_0^{\theta/2} ((2\pi)^{1/2} s)^{-1} \exp(-(\beta - \bar{\beta})^2/(2s^2))\, d\beta \times \int_{r_{min}}^{r_s} \lambda e^{-\lambda r}\, dr \qquad (15)$$

where the average cavity density $\bar{N}$ is based on the

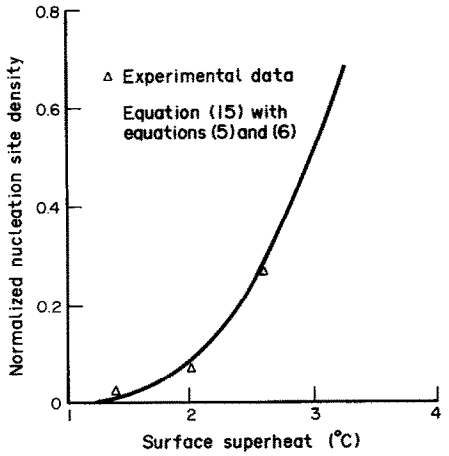

FIG. 9. Active nucleation site density vs superheat with equations (5) and (6) and experimental data.

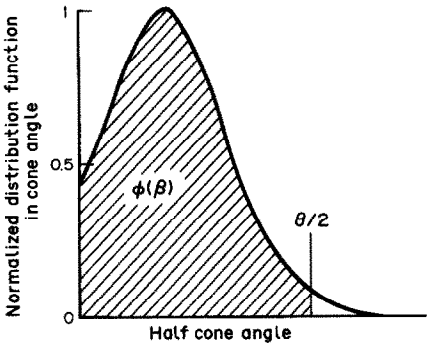

FIG. 10. Distribution function of cavity cone angle with equation (6).

measured data and it only depends on the boiling surface material and finish.

Actually, the contact angle θ and the surface tension σ can vary along with temperature [29]. The calculation of $\phi(\beta)$ and $\phi(r)$ indicates that when the contact angle varies by 1°, the variation of $\phi(\beta)$ is about 1%, but $\phi(r)$ almost does not change. Suppose the stainless steel–water combination has the same, or very close to the same value of $\Delta\theta/\Delta T = 0.1$ (this value corresponds to water–copper [29]), then when the superheat variation is about 10°C, the variation of $\phi(\beta)$ and $\phi(r)$ caused by contact angle variation is 1% and 0, respectively. From equation (15), the variation of surface tension does not affect the value of $\phi(\beta)$ and the effect of it on $\phi(r)$ is less than the effect of contact angle on $\phi(\beta)$. That is, surface tension actually does not affect both $\phi(r)$ and $\phi(\beta)$. Therefore, the above consideration leads to the fact that the active nucleation site density only depends on superheat for a given liquid–surface combination and the solid curve shows a normalized nucleation site density vs the surface superheat ΔT for the stainless steel–water specimen surface conditions with equations (5), (6) and (15) in Fig. 9.

DISCUSSION

In order to verify the dependence of N on ΔT (Fig. 9), a heating device which is similar to that of Porchey *et al.* [6] was designed and used. A temperature controller was used to adjust the boiling surface temperature. The surface superheat ΔT was changed as desired. Under several values of ΔT, the number of bubbles was observed on the area of the boiling surface under investigation. These results were compared with the result of equation (15). The temperature difference between the bulk of the water and the boiling surface was measured and then the corresponding active nucleation site density was computed by using the data acquisition system described in ref. [31].

After setting surface temperatures and confirming a steady state, on the monitor of the data acquisition system the number of bubbles were counted visually. In this way, the results were plotted in Fig. 9. When the temperature difference is over 2.6°C, it is difficult to determine the number of bubbles visually. But in the smaller temperature difference range, the agreement between equation (15) and the experiment is good, but a further data observation is needed with a better bubble counting technique.

It is interesting to look at equation (15) and compare it with the results provided by other investigators.

(1) Equation (15) indicates that the nucleation site density depends on the liquid–surface combination of the values of σ and θ. The effect of surface condition on nucleation site density is characterized by $\bar{N}$ and parameters such as the standard deviation s, mean $\bar{\beta}$, $\bar{\lambda}$ and r, which are included in the probability density function. So, most of the factors affecting the boiling heat transfer have been included in the model of equation (15), which is based on the surface geometric parameters measured by the SEM and DIC techniques.

(2) Figure 10 shows that the decreasing contact angle will reduce the value of $\phi(\beta)$ the shaded area, with $\phi(r)$, Fig. 11 being virtually unchanged, and as a result, the active nucleation site density will be reduced. Here

$$\phi(\theta) = \int f(\beta)\,\mathrm{d}\beta$$

is plotted for the varying cone angle in Fig. 10 in accordance with equation (6). The value of $\phi(r)$ of equation (5) represents the curve as the mouth radius of the cavity in μ changes from 0.4311 to 3.0175. Since the dynamic contact angle is less than the static contact angle [2], consideration of dynamic effects will decrease the active nucleation site density. This inference is consistent with the result of Singh *et al.* [32].

(3) Generally speaking, for most of the liquid and the technical grade metal surface combinations, the ratio of r_{max}/r_s is always greater than 1. This means that the factor for determining the value of $\phi(r)$ is r_s, not r_{max}, so the parameters, such as surface tension,

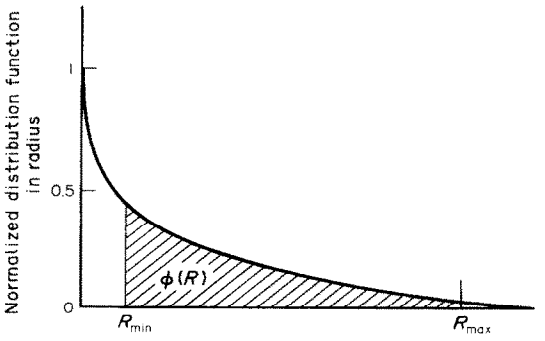

FIG. 11. Distribution function of cavity radius with equation (5) and its integral.

contact angle and cone angle could not have much effect on the value of $\phi(r)$. Furthermore, r_{max}/r_s is much greater than 1 for some liquid–surface combinations, e.g. water–stainless steel. In this case, the entrapping radius is considered infinite as suggested by Rohsenow [12].

(4) For a given liquid–surface combination, equation (15) is approximated as

$$N = \bar{N}\phi(\beta)\,e^{-\lambda r_{min}} = C e^{-K/\Delta T} \qquad (16)$$

where $C = \bar{N}\phi(\beta)$ is a constant for a given liquid–surface combination and $K = 2\sigma T_{sat} v_{fg}/h_{fg}$ is a constant for the given liquid–surface.

Equation (16) has the same mathematical form as that given by Gaertner and Westwater [11], but the difference lies in the constants which have a completely different meaning. Equation (16) is based on the clear understanding of the geometric characteristics of the boiling surface which are derived from statistical analysis.

CONCLUSION

(1) The description of the effect of heating surface conditions on the active nucleation site density is more suitable from boiling characteristics than from roughness alone. The boiling characteristics of the heating surface are surface cavity geometric parameters, mouth radius and cone angle, the distribution parameters, λ and s, and the average cavity density which is measurable by the SEM and DIC.

(2) Although the particular cavity distribution function that is in terms of the mouth radius and cone angle may vary along with the material and the surface finish, the measuring method and data processing technique can be used for other materials and different surface finishes.

(3) The upper limit of the active nucleation site radius is determined from equation (12), with its lower limit being given by equation (2). In some liquid–surface combination, the upper limit computed by equation (12) is much greater than the maximum cavity radius for common technical grade metal.

(4) The general relation between the active nucleation site density and the heating surface characteristics is expressed by equation (15) which has been derived from statistical considerations.

Acknowledgement—This project was supported by College of Engineering, University of North Carolina at Charlotte.

REFERENCES

1. C. Corty and A. S. Foust, Surface variables in nucleate boiling, *Chem. Engng Prog. Symp. Ser.* **51**, 50–60 (1962).
2. P. Griffith and G. D. Wallis, The role of surface conditions in nucleate boiling, *Chem. Engng Prog. Symp. Ser.* **56**, 49–63 (1960).
3. H. B. Clark, P. Strenge and J. Westwater, Active center in nucleate boiling, *Chem. Engng Prog. Symp. Ser.* **55**, 103–121 (1959).
4. K. Cornwell, *Lett. Heat Mass Transfer* **4**, 63–72 (1977).
5. M. Sultan and R. L. Judd, Spatial distribution of active sites and bubble flux density, *Trans. ASME, J. Heat Transfer* **100**, 56–62 (1978).
6. D. V. Porchey, E. L. Park, Jr. and K. G. Mayhan, A scanning electron microscope surface study of nucleate pool boiling heat transfer to saturated liquid nitrogen, *A.I.Ch.E. Symp. Ser.* **68**, 162–171 (1971).
7. J. P. Nail, Jr, R. I. Vachon and J. Morehouse, SEM study of nucleate sites in pool boiling from 304 stainless steel, *Trans. ASME, J. Heat Transfer* **96**, 132–137 (1974).
8. I. Z. Kopp, New model of nucleation in the boiling of liquids, *Heat Transfer—Sov. Res.* **13**, 117–125 (1981).
9. S. I. Vaynshteyn, A. F. Gandel'sman, E. E. Shpil'rayn, K. A. Yakimovich and I. Z. Kopp, Experimental unit for the study of condensing ejectors operating on mercury, *Heat Transfer—Sov. Res.* **13**, 8–16 (1981).
10. R. F. Gaertner, Distributions of active sites in nucleate boiling of liquids, *Chem. Engng Prog. Symp. Ser.* **59**, 52–61 (1963).
11. R. F. Gaertner and J. W. Westwater, Population of active sites in nucleate boiling heat transfer, *Chem. Engng Prog. Symp. Ser.* **56**, 39–48 (1960).
12. W. M. Rohsenow, Nucleation with boiling heat transfer, ASME Paper No. 70-HT-10 (1970).
13. D. Gorenflo, J. Goetz and K. Bier, Proposal of a standard apparatus for the measurement of pool boiling heat transfer, *Wärme- und Stoffübertr.* **16**, 69 (1982).
14. E. U. Schlünder, Heat transfer by boiling liquids, *Verfahrenstechnik* **4**, 493–497 (1970).
15. K. Bier, D. Gorenflo, M. Salem and Y. Tanes, Pool boiling heat transfer and size of active nucleation centers for horizontal plates with different roughness, *Proc. 6th Int. Heat Transfer Conf.*, Toronto, Vol. 1, pp. 151–156 (1978).
16. S. G. Bankoff, Entrapment of gas in the spreading of a liquid over a rough surface, *A.I.Ch.E. Jl* **4**, 24–26 (1958).
17. J. J. Lorenz, The effects of surface conditions on boiling characteristics, Ph.D. Thesis, Massachusetts Institute of Technology, Cambridge, Massachusetts (1971).
18. M. Shoukri and R. L. Judd, Nucleation site activation in saturated boiling, *Trans. ASME, J. Heat Transfer* **97**, 93–98 (1975).
19. Y. Y. Hsu, On the size range of active nucleation cavities on a heating surface, *Trans. ASME, J. Heat Transfer* **84**, 207–216 (1962).
20. K. Mizukami, Entrapment of vapor in re-entrant cavities, *Lett. Heat Mass Transfer* **2**, 279–284 (1975).
21. W. T. Brown, Jr., A study of flow surface boiling, Ph.D. Thesis, Massachusetts Institute of Technology, Cambridge, Massachusetts (1967).
22. R. L. Judd and M. Shoukri, Nucleate boiling on an oxide coated glass surface, *Trans. ASME, J. Heat Transfer* **97**, 494–495 (1975).
23. B. B. Mikic and W. M. Rohsenow, A new correlation of pool boiling data including the effect of heating surface

characteristics, *Trans. ASME, J. Heat Transfer* **91,** 245 (1969).
24. J. J. Lorenz, B. B. Mikic and W. M. Rohsenow, Effect of surface conditions on boiling characteristics, *Heat Transfer 1974*, Vol. IV, *Proc. 5th Int. Heat Transfer Conf.*, Tokyo (1974).
25. G. Kocamustafaogullari and M. Ishi, Interfacial area and nucleation site density in boiling system, *Int. J. Heat Mass Transfer* **26,** 1377–1387 (1983).
26. C. J. Smithells, *Metals Reference Book*, 5th Edn, pp. 1030–1031. Butterworth, London (1976).
27. J. E. Fruend, P. E. Livermore and I. Miller, *Manual of Experimental Statistics*, p. 26. Prentice-Hall, Englewood Cliffs, New Jersey (1962).
28. A. B. Ponter, G. A. Davies, T. K. Ross and P. G. Thornley, The influence of mass transfer on liquid film breakdown, *Int. J. Heat Mass Transfer* **10,** 349–359 (1967).
29. A. B. Ponter, G. A. Davies, W. Beaton and T. K. Ross, The measurement of contact angles under conditions of heat transfer when liquid film breaks on a vertical surface, *Int. J. Heat Mass Transfer* **10,** 1633–1636 (1967).
30. I. Z. Kopp, Effect of surface roughness on boiling heat transfer, *Heat Transfer—Sov. Res.* **8,** 37–42 (1976).
31. R. H. Kim and S. R. Yang, Data acquisition system, *Proc. 31st Int. Instrumentation Symposium*, San Diego, California, Vol. 31, pp. 339–352 (1985).
32. A. Singh, B. B. Mikic and W. M. Rohsenow, Active sites in boiling, *Trans. ASME, J. Heat Transfer* **98,** 401–406 (1976).

UN MODELE MATHEMATIQUE DE LA DENSITE DE SITES DE NUCLEATION POUR L'EBULLITION EN RESERVOIR EN FONCTION DES CARACTERSTIQUES DE LA SURFACE

Résumé—La densité de sites de nucléation active est exprimée en fonction des conditions de la surface par la forme $N = N \cdot \phi(\beta) \cdot \phi(r)$. La densité moyenne de cavité N est obtenue à partir des mesures. Les fonctions de distribution $\phi(\beta)$ et $\phi(r)$ ont la forme

$$\phi(\beta) = \int_0^{\theta/2} f(\beta)\,\mathrm{d}\beta, \qquad \phi(r) = \int_{r_{\min}}^{r_{\max}} f(r)\,\mathrm{d}r.$$

La densité de probabilité du rayon de l'ouverture de cavité $f(r)$ et de l'angle du cône $f(\beta)$ sont obtenus par un traitement statistique portant sur les cavités mesurées par examen au microscope électronique et au microscope à contraste par interférence différentielle. L'accord est bon entre les résultats de l'analyse et ceux de l'expérience.

EIN MATHEMATISCHES MODELL ZUR BLASENKEIMSTELLENDICHTE BEIM BEHÄLTERSIEDEN IN ABHÄNGIGKEIT DER OBERFLÄCHENEIGENSCHAFTEN

Zusammenfassung—Die Abhängigkeit der Belegungsdichte aktiver Blasenkeimstellen von den Eigenschaften der Heizfläche wurde in der Form $N = N \cdot \phi(\beta) \cdot \phi(r)$ entwickelt. Die mittlere Keimstellendichte N wurde aus Messungen an der Siedeoberfläche ermittelt. Die Verteilungsfunktionen $\phi(\beta)$ und $\phi(r)$ haben die Form

$$\phi(\beta) = \int_0^{\theta/2} f(\beta)\,\mathrm{d}\beta; \quad \phi(r) = \int_{r_{\min}}^{r_{\max}} f(r)\,\mathrm{d}r.$$

Die Wahrscheinlichkeitsdichte-Funktionen des Öffnungsradius $f(r)$ und des Öffnungswinkels $f(\beta)$ der Vertiefungen wurden durch ein statistisches Verfahren ermittelt, das auf den mit einem Elektronen-Raster-Mikroskop und einem Differential-Interferenz-Kontrast-Mikroskop gemessenen Vertiefungen beruht. Die Grenzen der Integration sind durch den Einschlußmechanismus gegeben.

МАТЕМАТИЧЕСКАЯ МОДОЕЛЬ ДЛЯ ПЛОТНОСТИ ЦЕНТРОВ ПАРООБРАЗОВАНИЯ ПРИ КИПЕНИИ В БОЛЬШОМ ОБЬЕМЕ С УЧЕТОМ ХАРАКТЕРИСТИК ПОВЕРХНОСТИ

Аннотация—Выведена зависимость плотности активных центров парообразования от устлоний кипения на поверхности в виде $N = N \cdot \phi(\beta) \cdot \phi(r)$. Осредненная плотность распределения впадины получена в результате измерений на поверхности кипения. Функции распределения $\phi(\beta)$ и $\phi(r)$ имеют форму

$$\phi(\beta) = \int_0^{\theta/2} f(\beta)\,\mathrm{d}\beta, \qquad \phi(r) = \int_{r_{\min}}^{r_{\max}} f(r)\,\mathrm{d}r.$$

Функция плотности вероятности распределения радиуса устья впадин $f(r)$ и угол конусности $f(\beta)$ получены при статистической обработке измеренных впадин с помощью сканирующего электронного микроскопа и контрастного дифференциального интерференционного микроскопа. Соответствие между результатами анализа и экспериментальными данными является хорошим.